2. V. A. Derevyanko, V. S. Slavin, and V. S. Sokolov, "An MHD generator containing a T layer," Proceedings of the 8th Intern. Conference on MHD Energy Conversion [in Russian], Vol. 2, Moscow (1983).
3. J. M. Wetzer, "Microscopic and macroscopic streamer parameters of a noble gas linear MHD generator," 22nd Symposium on Engineering Aspects of MHD, Starkville, USA (1984).
4. S. V. Kukhtetskii, A. D. Lebedev, and V. A. Lyubochko, "Motion of a high-current discharge in a dense gas," Teplofiz. Vysok. Temp., 23, No. 3 (1985).
5. A. D. Lebedev, V. I. Nazaruk, et al., "A high-current arc discharge in a magnetic field," in: Low-Temperature Plasma Generators [in Russian], Part 1, Kaunas (1986).
6. J. C. N. Bosma, A. Veefkind, J. F. Uhlenbuch, and L. H. Rietjens, "Experimental investigation on the gasdynamic interaction between streamers and background gas in a noble gas MHD generator," 23rd Symp. on Engineering Aspects of MHD, Pennsylvania (1985).
7. A. N. Tikhonov, A. A. Samarskii, et al., "The nonlinear effect in the formation of a self-maintaining hot conducting gas layer in nonstationary magnetohydrodynamics," Dokl. Akad. Nauk SSSR, 173, No. 4 (1967).
8. V. A. Derevyanko, V. S. Slavin, and V. S. Sokolov, "A magnetohydrodynamic electricity generator based on brown-coal gasification products," Zh. Prikl. Mekh. Tekh. Fiz., No. 5 (1980).
9. E. N. Vasil'ev, V. A. Derevyanko, and V. S. Slavin, "A stabilized current layer," Teplofiz. Vysok. Temp., 24, No. 5 (1986).
10. I. V. Nemchinov, "The averaged radiation-transport equations and applications in gasdynamic treatments," Prikl. Mat. Mekh., 34, No. 4 (1970).
11. I. A. Sokolova, "Transport coefficients and collision integrals for air and air components," in: Physical Kinetics [in Russian], ITPM SO AN SSSR, Novosibirsk (1974).
12. I. V. Avilova, L. M. Biberman, et al., The Optical Parameters of Hot Air [in Russian], Nauka, Moscow (1970).
13. V. A. Derevyanko, V. S. Sokolov, et al., "Experimental investigation of self-maintained current layer in MHD channel," 9th Intern. Conf. on MHD Electrical Power Generation, Tsukuba, Japan (1986), Vol. 4.
14. N. P. Gridnev, S. S. Katsnel'son, and V. P. Fomichev, Inhomogeneous MHD Flows Containing T Layers [in Russian], Nauka, Novosibirsk (1984).
15. N. V. Sosnin and A. P. Favorskii, Steady-State Magnetohydrodynamic T-Layer Structures [in Russian], No. 64, Preprint, Inst. Prikl. Mat. Akad. Nauk SSSR, Moscow (1976).
16. S. Trogott, "The radiative heat flux potential for a nongray gas," RTK, 4, No. 3 (1966).
17. E. N. Vasil'ev, V. V. Ovchinnikov, and V. S. Slavin, "The phase diagram for a stabilized current layer in an MHD generator channel," Dokl. Akad. Nauk SSSR, 290, No. 6 (1986).

SIMULATING THE CATHODE REGION IN A STATIONARY SELF-MAINTAINED GLOW DISCHARGE

V. A. Shveigert and I. V. Shveigert

UDC 537.52

The cathode region is the most important part of a gas discharge as it is responsible for the very existence of it [1]. The electric fields are strong and highly inhomogeneous there, and consequently there is a nonlocal relation between the electron distribution and the field strength [2], which substantially complicates examining that region. At present, there is no self-consistent analysis for that region that incorportes the nonlocal electron distribution and the relations between the various parts of the cathode region: the cathode layer, the negative glow, and the Faraday dark space. In [3, 4], the layer was examined most fully, but the discussion concerned short discharge gaps, where there is virtually no weak-field region. Here we present a model that treats the cathode region in a self-consistent fashion. The results are briefly compared with ones for discharges in helium.

We consider the case of low cathode potential differences ($U_c \leqslant 500$ V) and medium gas-atom concentrations ($N \sim 10^{16}$-10^{17} cm^{-3}), for which one can neglect the participation of fast ions and neutral particles (in direct ionization, as well as kinetic electron ejection from

Novosibirsk. Translated from Zhurnal Prikladnoi Mekhaniki i Tekhnicheskoi Fiziki, No. 4, pp. 16-23, July-August, 1988. Original article submitted March 12, 1987.

0021-8944/88/2904-0471$12.50

the cathode), in addition to gas heating, stepwise processes, and so on. Charged particles are produced in the gas volume by electrons colliding with gas atoms in the ground state, while they are lost by transfer to the electrodes and walls. Then the cross section for the formation of a k-charged ion species decreases approximately as $1/I_k^2$ (I_k is the ionization potential [5]), so the proportion of highly charged ions ($k \geqslant 2$) is small, which is confirmed by measurements [6]. Electrons are generated at the cathode by potential ion-electron emission, coefficient γ_i independent of ion energy [7].

The discharge is described by Poisson's equation for the electric field potential φ together with the kinetic equations for the electron and singly-charged atomic ion distributions. Symmetrical charge transfer is the basic process in ion scattering in the same gas [5], while the ion mean free path at low U_c is much less than the cathode-layer thickness. Therefore, the ion motion is described satisfactorily in the diffusion-drift approximation [8], as is confirmed by calculations on ion distributions [9].

Monte Carlo methods are the most economical [2] for calculating electron distributions in highly inhomogeneous fields. The speed in the low-field region is much reduced, and simulating low-energy electron paths there can consume much computer time. Also, major difficulties arise in providing a self-consistent solution to the entire equation system for a quasineutral plasma. Therefore, up to now, it has not been possible to calculate or explain electron distributions for weak-field regions [1, 10]. Measurements [11, 12] show that in such regions, the electrons can be divided into three groups: primary ones, whose energies are above the atomic excitation threshold, secondary ones having energy about 5-10 eV, and final ones having temperature $T_e \approx 1$ eV (the concentrations are n_p, n_s, and n_f correspondingly). The primary electrons acquire energy in the cathode layer and are responsible for ionizing and exciting the gas in the low-field region, while the conductivity is completely determined by the final electrons ($n_f \gg n_s \gg n_p$) [13].

The energy lost by the primary electrons in inelastic processes in the low-field region exceeds the energy acquired in the electric field. The fast-electron concentration decreases exponentially in the negative glow. A group of secondary electrons is produced whose energies are less than the atomic excitation potential. These energies relax in elastic collisions having frequency ν_e and in electron–electron collisions having frequency ν_{ee}, in which $\nu_{ee} > 2m\nu_e/M$ (m and M are electron and atom masses). The mechanism responsible for energy exchange between the secondary and final electrons is not entirely clear [1]. The secondary-electron distribution is governed by the loss to the tube wall, since the potential barriers at the walls are not very high.

Estimates [1] give $\nu_{ee} \gg 2m\nu_e/M$ for the final electrons, since the electron–electron collision cross section is proportional to $1/\varepsilon^2$ (ε is electron energy), and the final-electron distribution is close to Maxwellian.

As the electrons can be divided into groups, one can use a hybrid model for the low-field region, in which the high-energy part of the electron distribution is described by a kinetic equation, while the low-energy one is described by the diffusion-drift approximation. The path of an electron starting from the cathode ($z = 0$) may be traced by Monte Carlo methods up to $z = z_*$. For $z > z_*$, the field strength is small, and the path can be simulated until the electron energy becomes less than the excitation threshold. The electron is then considered as a final one and as moving in the diffusion-drift approximation. The final-electron concentration includes the secondary-electron one. The final-electron temperature is not defined in this model but instead is specified as an external parameter, which has to be taken from experiment.

The following approximations are used in simulating the electron distribution: elastic scattering is isotropic, the direction of motion does not change in inelastic collisions, and the electrodes and walls are absolutely absorbing for the electrons. There is only a minor effect on the distribution from incorporating angular anisotropy in electron scattering [2].

We envisage a discharge in a tube for the case where the most measurements are available on the cathode region. Such measurements [14] show that the radial charged-particle concentration profile is closely described by a zero-order Bessel function, so one can use a one-dimensional model by introducing the effective time for charged-particle loss to the wall, $1/\tau_a = D_a(2.4/R)^2$ (D_a is the ambipolar diffusion coefficient and R is tube radius). In most two-dimensional models (axial symmetry assumed) [1, 10], the variables are separated to reduce the treatment to one-dimensional cases. In [15], the plasma in the weak-field region

was described in the quasineutrality approximation by means of a purely two-dimensional model, but the high-energy electron distribution was specified phenomenologically.

With these approximations, the expanded equation system is

$$\frac{\partial^2\varphi}{\partial z^2} = 4\pi e(n_e - n_i),\ E = -\frac{\partial\varphi}{\partial z},\quad n_e = n_f + n_p; \tag{1}$$

$$-\frac{\partial}{\partial z}\left(\mu_e E n_f + D_e\frac{\partial n_f}{\partial z}\right) = S_i - \frac{n_f}{\tau_a}; \tag{2}$$

$$-\frac{\partial}{\partial z}\left(-\mu_i E n_i + D_i\frac{\partial n_i}{\partial z}\right) = S_i - \frac{n_i}{\tau_a}; \tag{3}$$

$$v\mu\frac{\partial\psi}{\partial Nz} + v\sqrt{1-\mu^2}\left(\cos\theta\frac{\partial\psi}{\partial Nx} + \sin\theta\frac{\partial\psi}{\partial Ny}\right) - \frac{eE}{N}\left(\frac{1}{p}\frac{\partial}{\partial\mu}(1-\mu^2)\psi + \mu\frac{\partial}{\partial\varepsilon}v\psi\right) = -\sum v\psi +$$

$$+\frac{1}{2}\int_0^{2\pi}\sigma_{tr}(\varepsilon+\delta\varepsilon)\,v(\varepsilon+\delta\varepsilon)\,\psi(\varepsilon+\delta\varepsilon,\mu,\theta)\,d\mu +$$

$$+2\int_{\varepsilon+I}^{\infty}\sigma_i(\varepsilon')\,v(\varepsilon')\,\psi(\varepsilon')\,W(\varepsilon,\varepsilon')\,d\varepsilon' + \sum_k\sigma_k(\varepsilon+\Delta\varepsilon_k)\,v(\varepsilon+\Delta_k)\,\psi(\varepsilon+\Delta\varepsilon_k) -$$

$$-\frac{v\psi}{l},\ n_p = \langle\psi\rangle,\ S_i = \langle\sigma_i v\psi\rangle,\ S_t = \left\langle\frac{v}{l}\psi\right\rangle,\quad \Sigma = \sigma_{tr} + \sigma_i + \sum_k\sigma_k. \tag{4}$$

We now consider the boundary conditions. Electrons starting from the cathode were traced by Monte Carlo methods, and the final-electron current at the cathode was zero: $\mu_e E n_c + D_e\partial n_c/\partial z|_{z=0} = 0$. The ion motion in the cathode dark space is of messenger type. When an ion collides with a neutral atom, charge is transferred, and a fast neutral atom is formed along with an almost immobile ion, which begins to be accelerated. The ion motion is calculated in the diffusion-drift approximation subject to the boundary condition $\partial n_i/\partial z|_{z=0} = 0$, which has given good agreement with calculations on the motion by Monte Carlo methods [16]. The ion diffusion is unimportant in the strong-field region, since the drift velocity greatly exceeds the thermal value (ion temperature T_i equal to the gas temperature T_g). The boundary conditions for the ions at the cathode has an effect only via the diffusion term and can be fairly arbitrary.

The hydrodynamic boundary conditions at the anode $n_c|_{z=d} = 0$, $n_i|_{z=d} = 0$ [17] enable one to describe the entire gap correctly apart from the anode layer, whose thickness is of the order of the electron and ion mean free paths. The usual boundary conditions are applied for the potential: $\varphi|_{z=0} = 0$, $\varphi|_{z=d} = U_p$.

Measurements [18, 19] give the secondary-electron distribution at the cathode as approximated by

$$\psi(z=0, x, y, \varepsilon, \mu, \theta) = \begin{cases} A\mu\sin(\pi\varepsilon/(I-2\delta\varphi)), & \varepsilon < I - 2\delta\varphi, \\ 0, & \varepsilon > I - 2\delta\varphi. \end{cases}$$

Here A is defined by

$$\frac{1}{2}\int_0^{\infty}d\varepsilon\int_0^{2\pi}d\theta\int_0^{1}\mu v\psi\,d\mu\,|_{z=0} = \gamma_i\mu_i E n_i\,|_{z=0}.$$

In (1)-(4), σ_{tr} is the transport scattering cross section, n_e, n_i, μ_e, μ_i, D_e, D_i are the electron and ion concentrations, mobilities, and diffusion coefficients, S_i and S_t are the ionization rate and the primary-electron thermalization rate, σ_i and σ_k are the ionization and excitation cross sections for level k, I and $\Delta\varepsilon_k$ are the ionization potential and excitation energy for level k, d electrode separation, U_p potential drop across discharge, $\delta\varphi$ electron work function at cathode, ε, p, and v electron energy, momentum, and velocity, $\delta\varepsilon = 2m/M(1-\cos\eta)\varepsilon$ (η is scattering angle), $W(\varepsilon', \varepsilon)$ the probability of producing an electron having energy ε on ionization $\left(\int_0^{\varepsilon-I}W(\varepsilon',\varepsilon)\,d\varepsilon = 1\right)$, $(1/2)\psi(\varepsilon,\mu,\theta,r)d\varepsilon\,d\mu\,d\theta$ the number of electrons in the phase interval $(1/2)d\varepsilon d\mu d\theta$, μ the cosine of the angle between the electron velocity and the Oz axis, θ the angle between the Ox axis and the electron velocity component transverse to the field, and $\ell = \lambda/10$ (λ is electron mean free path for plastic collisions).

A different description has been given for the high-energy part of the distribution for weak fields [20, 21] and has been used in the theoretical analysis of negative glows [1, 10]. (1)-(3) were solved in the quasineutrality approximation:

$$-\frac{\partial^2 n_i}{\partial z^2}=\frac{S_i}{D_a}-\frac{n_i}{\tau_a D_a},\quad E=-\frac{j-j_p}{\mu_e n_i}-T_e\frac{\partial \ln n_i}{\partial z} \tag{5}$$

(j and j_p are the discharge-current and primary-electron densities). The condition $n_i = n_0$ was imposed at the boundary between the cathode layer and the negative glow, where n_0 was either taken from experiment or set as zero. The ionization-rate and primary-electron current-density distributions were specified phenomenologically, usually as exponentially decreasing towards the anode [22].

(1)-(4) enable one to avoid these approximations and to consider the discharge structure in a self-consistent fashion (with known μ_e, D_e), and as the electron thermal conductivity is substantially larger than the ambipolar diffusion coefficient (by a factor μ_e/μ_i), the final-electron temperature T_e varies over the discharge gap much less than does the concentration [11, 23], and so μ_e, D_e may be taken as constant: $N\mu_e = 3.54\cdot10^{22}$ $(\text{sec}\cdot\text{cm}\cdot\text{V})^{-1}$ [24] and $D_e = \mu_e T_e$. Qualitative examination of (5) and numerical calculations [9] show that the error in specifying T_e has only a slight effect on the discharge parameters in the strong-field region, although (5) shows that any reduction in the final-electron temperature should result in an increased concentration for an unaltered spatial distribution. Correspondingly, the field strength in the weak-field region decreases as T_e falls. Therefore, (1)-(4) do not incorporate ionization by the final electrons, and so that model does not describe the transition from the Faraday dark space to the positive column.

The algorithm used in the electron-distribution simulation has been described in detail [2]. The ionization cross sections were taken from [25] and $W(\varepsilon', \varepsilon)$ from [26], with the scattering transport cross section from [2] and $\delta\varphi = 4.5$ eV. The set of actual electronic states in helium was replaced by the metastable level ($\Delta\varepsilon_1 = 19.82$ eV) and an effective level ($\Delta\varepsilon_2 = 21.45$ eV), which combined the other levels [27]. The excitation cross sections were taken as in [27]. Test calculations on a linearly decreasing field gave good agreement with the [2] results, where 22 levels were incorporated for helium in the latter. A monotone conservative Scharfetter–Gummel scheme [28] was used to solve (2) and (3), which gave good accuracy for high gradients. The nonlinear difference-equation system corresponding to (1)-(3) was solved by Newton's method with vector fitting. The [8] approximations were used for μ_i and D_i. We set z_* at the left-hand boundary of the weak-field region, which had little effect on the results. In [4], various algorithms have been discussed for self-consistent solution of (1)-(4). Here we fixed γ_i and used the following method. With a given secondary-electron current at the cathode, simple iterations (usually two or three) were used to solve (1)-(4) and derive the coefficient γ_i' relating the ion and electron currents at the cathode. Then the secondary-electron current at the cathode was adjusted to make γ_i' correspond to γ_i. The error in the iterations for producing γ_i consistent to 10% was within the statistical error limits in the Monte Carlo method, where we usually employed about $(3\text{-}10)\cdot10^3$ paths. The total time required to calculate one form of model with the BÉSM-6 was 1-2 h.

A fairly detailed study has been made [2] on the electron distribution in helium for a linearly decreasing field. We show below that this approximation agrees well with self-consistent calculations, so here we consider only the agreement between theory and experiment for the high-energy part in the weak-field region. Measurements have been made [2] on the electron distributions in helium at the anode for various distances from the cathode, and the theoretical distributions (a and b) and the observed one (c) are shown in Fig. 1 for $p = 2\cdot10^3$ Pa, $d = 0.1$ cm, $U_p = 200$ V, $j = 8\cdot10^{-3}$ A/cm^2, and $R \approx 0.6$ cm. The measurements were made with a potential difference of 270 V, but about 70 V was accounted for by the anode potential drop due to an insulating film on the anode [29], so according to [29], the measured distribution was displaced 70 V along the axis. In these calculations, U_p and j_i were fixed on the basis that high-energy electrons ($\varepsilon > 50$ eV) are scattered back from the anode with the reflection coefficient from [30]. The secondary-emission coefficient obtained in the self-consistent calculation was 0.25. We are not aware of any measurements on γ_i for helium ions with the steel cathode used in the measurements. For comparison, $\gamma_i(T_a) = 0.14$ [31], $\gamma_i(W) = 0.29$ [32], $\gamma_i(N_i) = 0.16$ [33] for atomically clean surfaces. Figure 1 shows satisfactory agreement between theory and experiment. A characteristic feature of the distribution is that there is an isolated electron group whose energy exceeds the potential difference between the electrodes, which persists with other discharge parameters. The electrons

TABLE 1

Model number	j, A/cm²	U_p, V	E_c, V/cm	dc, cm	d_s, cm	N_c, %	N_s, %	M_e	M_i	N_i, %
1	$2{,}55\cdot10^{-6}$	237	156	2,83	2,26	24	120	11,7	7,46	100
2	$1{,}28\cdot10^{-5}$	270	319	1,55	1,42	15	175	10,4	9,03	93
3	$6{,}38\cdot10^{-5}$	370	648	0,88	1,08	8	160	9,0	11,4	78

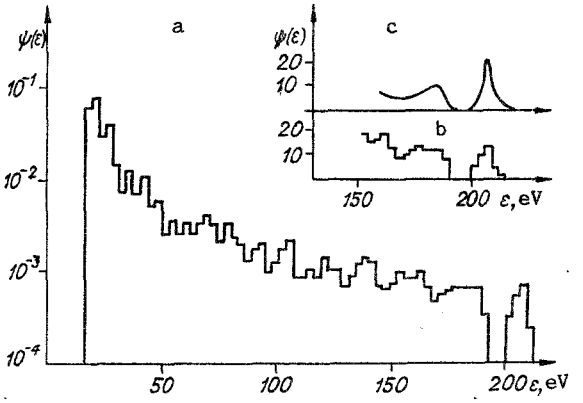

Fig. 1

in this group do not undergo any inelastic collisions in the gap and the characteristic energy spread $\sim I - 2\delta\varphi$ is determined by the secondary-electron distribution at the cathode. Most of the electrons show at least one inelastic collision. At 50-190 eV, the distribution falls comparatively slowly as the energy increases, which agrees with the measurements [29].

Measurements have been made on the field distribution in helium with an anomalous discharge [34] at p = 13-133 Pa in a tube 10 cm in diameter and 40 cm long. The (1)-(4) model does not describe the positive column, so the electrode gap was taken shorter than the actual value (d = 5 cm). It was assumed that the anode position does not affect the parameters for the cathode layer and negative glow. Secondary-emission coefficient 0.12, gas pressure 133 Pa. T_e was not measured in [34]. Also, T_e is only slightly dependent on the current density [35] and increases as the gas pressure and tube radius decrease, while the characteristic range is 0.04-0.6 eV. We assumed T_e = 0.4 eV. When T_e increases by a factor five, the cathode-layer parameters alter by amounts lying within the self-consistent errors (U_c and cathode field E_c). The comparison with experiment was at identical current densities.

Table 1 gives some calculations: N_s the number of fast electrons reaching the wall, d_c the cathode layer thickness obtained on interpolating the field to zero, d_s the position for the maximum gas excitation rate, N_c the proportion of electrons back-scattered at the cathode, M_e and M_i the numbers of excitations and ionizations in the bulk, N_i the proportion of ions

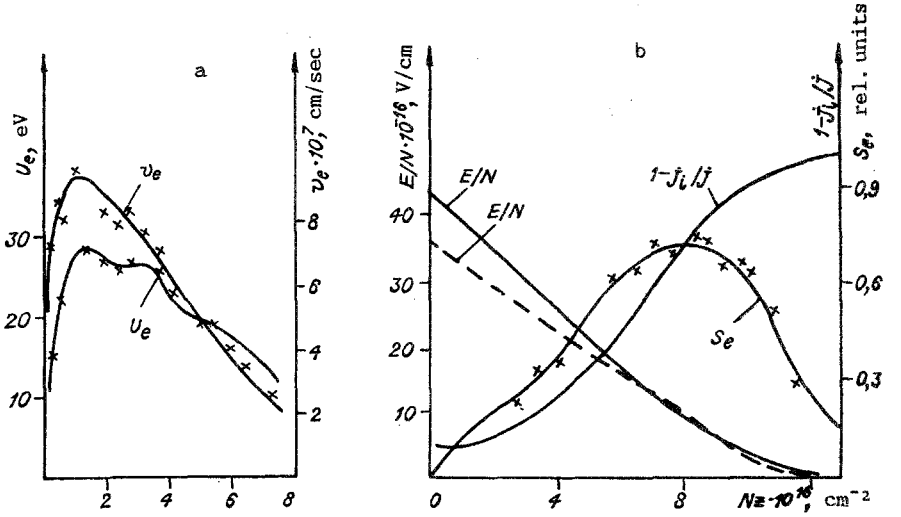

Fig. 2

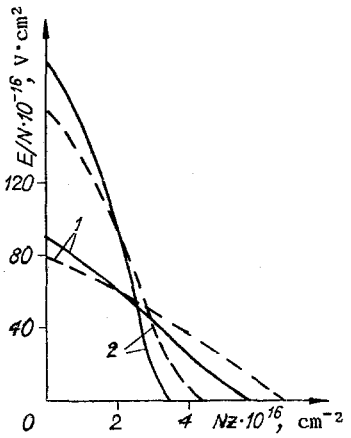

Fig. 3

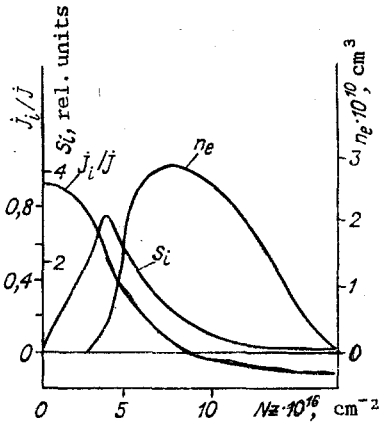

Fig. 4

arriving at the cathode, where N_s, M_e, and M_i have been calculated per electron leaving the cathode.

At the lowest current densities (model 1) used in the measurements, the cathode potential drop was close to normal. Figure 2a (model 1) shows that the mean v_e and U_e (speed and energy for the electrons in the cathode layer) are nonlocally dependent on the field in the slightly anomalous state. The negative glow corresponding to the maximum gas excitation rate S_e (Fig. 2b) lies in the high-field region, so one cannot artificially divide the cathode region into the cathode dark layer and negative glow, as has previously been done in describing these regions separately, in the case of slightly anomalous states. The spatial distribution for the ion current density j_i (Fig. 2b) shows that almost all the ions are generated in the high-field region and arrive at the cathode (Table 1). The measured (dashed line) and calculated (solid line) electric field distributions are close to linear, with the maximum difference between theory and experiment (about 20%) occurring at the cathode (Fig. 2, here and subsequently we give the absolute fields).

There is good agreement between theory (solid line) and experiment (dashed line) as the current density increases (Fig. 3, where curve 1 is for model 2 and curve 2 for model 3). In the anomalous state, the negative glow is displaced to the weak-field region. The S_i profile (Fig. 4, model 3) is close to that for the excitation rate, and many of the ions are generated in the weak-field region, although only some of them reach the cathode. For U_p = 370 V, about half the ions reach the cathode from the weak-field region (Fig. 4, j_i distribution). The electron concentrations in the weak-field region have the peak familiar from experiment [10], which is approximately proportional to the final-electron temperature. The field changes sign in the negative glow, and an electron potential well is formed, whose depth is proportional to T_e.

LITERATURE CITED

1. V. A. Granovskii, Electric Currents in Gases: Steady-State Current [in Russian], Nauka, Moscow (1971).
2. J. P. Boeuf and E. Marode, "A Monte Carlo analysis of an electron swarm in a nonuniform field: the cathode region of a glow discharge in helium," J. Phys. D: Appl. Phys., 15, 2169 (1982).
3. P. Segre, M. Yousfi, and E. Marode, "A self-consistent microscopic study of the cathodic zone of a helium–mercury discharge," 6th Int. Conf. Gas Discharges and Their Appl., Edinburgh (1980), Part 2.
4. J. P. Boeuf, E. Marode, et al., "Electron and ion behaviour in the cathode region of a discharge studied by Monte Carlo techniques," 6th Int. Conf. Gas Discharges and Their Appl., Edinburgh (1980), Part 2.
5. B. M. Smirnov, Ions and Excited Atoms in Plasmas [in Russian], Atomizdat, Moscow (1974).
6. A. V. Bondarenko, "A mass and energy analysis for ions in the cathode region of an anomalous glow discharge," Zh. Tekh. Fiz., 43, No. 4 (1973).
7. M. Kaminski, Atomic and Ionic Impact Phenomena on Metal Surfaces, Springer-Verlag, New York (1965).
8. E. McDaniel and E. Mason, Mobility and Diffusion of Ions in Gases, Wiley, New York (1973).

9. G. V. Gadiyak, K. A. Nasyrov, V. A. Shveigert, and O. U. Uuemaa, Simulating Gas-Discharge Lasers [in Russian], Preprint No. 30-80, ITPM SO AN SSSR, Novosibirsk (1985).
10. M. S. Blinderman, The Cathode Parts of a Glow Discharge: Current State of Research [in Russian], Preprint No. 216, Inst. Problem Mekhaniki, Moscow (1983).
11. D. H. Pringle and W. E. J. Farvis, "Electron groups in the helium negative glow," Phys. Rev., 96, 836 (1955).
12. J. M. Anderson, "Ultimate and secondary electron energies in the negative glow of a cold-cathode discharge in helium," J. Appl. Phys., 31, 511 (1960).
13. G. Franck and E. Schlosser, "Elektronengruppen, ihre Temperaturen und Dichten im diffusion- und recombinationsbestimmten H_2-Glimmlicht," Z. Physik, 224, 222 (1969).
14. G. A. Woolsey, R. M. Reynolds, et al., "The negative flow and Faraday dark space in near-normal discharges," Int. J. Electr., 26, 505 (1969).
15. A. Heisen and B. Wunderer, "Eine phenomenologische Theorie des negativen glimmlichtsanomalen Glimmentladungen unter Berücksichtigung der Volumenrekombination," Z. Physik, 224, 237 (1969).
16. V. A. Shveigert and I. V. Shveigert, "The cathode region in a glow discharge in an inert gas," in: High-Power CO_2 Lasers for Plasma Experiments and Technology [in Russian], Novosibirsk (1986).
17. I. V. Chekmarev, "Thermal boundary conditions for electrons in a weakly ionized gas around a catalytic wall," Zh. Tekh. Fiz., 51, No. 8 (1981).
18. H. D. Hagstrum, "Theory of Auger ejection of electrons from metals by ions," Phys. Rev., 96, 336 (1954).
19. R. C. Abbot and H. W. Berry, "Measurement of the angular distribution of electrons ejected from tungsten by helium ions," J. Appl. Phys., 30, 871 (1959).
20. W. Weizel, R. Rompe, and M. Schon, "Theorie der kathodischen Entladungsteile einer Niederdruckentladung. II. Das Glimmlicht," Z. Physik, 133, 87 (1939).
21. O. Scherzen, "Theorie der Glimmentladung," Arch. Elektrotechn., 33, 207 (1939).
22. J. Welhelm and W. Kind, "Zur Theorie des Glimmlichts einer Niederdruckentladung," Beitr. Plasmaphys., 5, 395 (1965).
23. G. S. Solntsev, A. I. Orlov, and V. A. Dovzhenko, "The mechanism governing the electron-energy distribution in a negative glow-discharge plasma," Radiotekh. Radioelektron., 15, No. 9 (1970).
24. A. L. Ward, "Calculations of cathode-fall characteristics," J. Appl. Phys., 83, 2789 (1962).
25. D. Rapp and P. Englander-Golden, "Total cross sections for ionization and attachment in gases by electron impact. 1. Positive ionization," J. Chem. Phys., 43, 464 (1965).
26. A. E. S. Green and T. Sawada, "Ionization cross sections and secondary electron distribution," J. Atmos. Terr. Phys., 34, 1719 (1972).
27. Tran Ngoc An, E. Marode, and P. C. Johnson, "Monte Carlo simulation of electrons within the cathode fall of a glow discharge in helium," J. Phys. D: Appl. Phys., 10, 2317 (1977).
28. D. L. Scharfetter and H. K. Gummel, "Large-signal analysis of a silicon read diode oscillator," IEEE Trans. Electr. Dev., ED-16, No. 1 (1969).
29. P. Gill and C. E. Webb, "Electron energy distributions in the negative glow and their relevance to hollow cathode lasers," J. Phys. D: Appl. Phys., 10, 299 (1977).
30. I. K. Kikoin (ed.), Tables of Physical Quantities [in Russian], Atomizdat, Moscow (1976).
31. H. D. Hugstrum, "Electron ejection from Mo by He^+, He^{++}, He_2^+," Phys. Rev., 89, 244 (1953).
32. H. D. Hugstrum, "Auger ejection of electrons from molybdenum by noble gas ions," Phys. Rev., 104, 672 (1956).
33. Y. Takeishi, "A note on the normal cathode fall in the glow discharges in inert gases," J. Phys. Soc. Jpn., 13, 767 (1958).
34. R. Warren, "Field measurement in glow discharges with a refined electron beam probe and automatic recording," Phys. Rev., 98, 1650 (1955).
35. G. Franck, K. Held, and H. D. Pfeil, "Velocity distribution of plasma electron in the negative H_2- and He-glow with superimposed longitudinal magnetic field," Z. Physik, 256, 73 (1972).